

Room temperature growth of h-BN nanosheets by pulsed laser deposition

Abhijit Biswas^{1,7*}, Rishi Maiti^{2,7}, Frank Lee^{3,7}, Cecilia Y. Chen⁴, Tao Li⁵, Anand B. Puthirath¹, Sathvik Ajay Iyengar¹, Chenxi Li¹, Xiang Zhang¹, Harikishan Kannan¹, Tia Gray¹, Md Abid Shahriar Rahman Saadi¹, Jacob Elkins¹, A. Glen Birdwell⁶, Mahesh R. Neupane⁶, Pankaj B. Shah⁶, Dmitry A. Ruzmetov⁶, Tony G. Ivanov⁶, Robert Vajtai¹, Yuji Zhao⁵, Alexander L. Gaeta^{2,4*}, Manoj Tripathi^{3*}, Alan Dalton³ and Pulickel M. Ajayan^{1*}

¹Department of Materials Science and Nanoengineering, Rice University, Houston, Texas 77005, USA.

²Department of Applied Physics and Applied Mathematics, Columbia University, New York, 10027, USA.

³Department of Physics and Astronomy, University of Sussex, Brighton BN1 9RH, United Kingdom.

⁴Department of Electrical Engineering, Columbia University, New York, 10027, USA.

⁵Department of Electrical and Computer Engineering, Rice University, Houston, TX, 77005, USA.

⁶DEVCOM Army Research Laboratory, RF Devices and Circuits, Adelphi, Maryland 20783, USA.

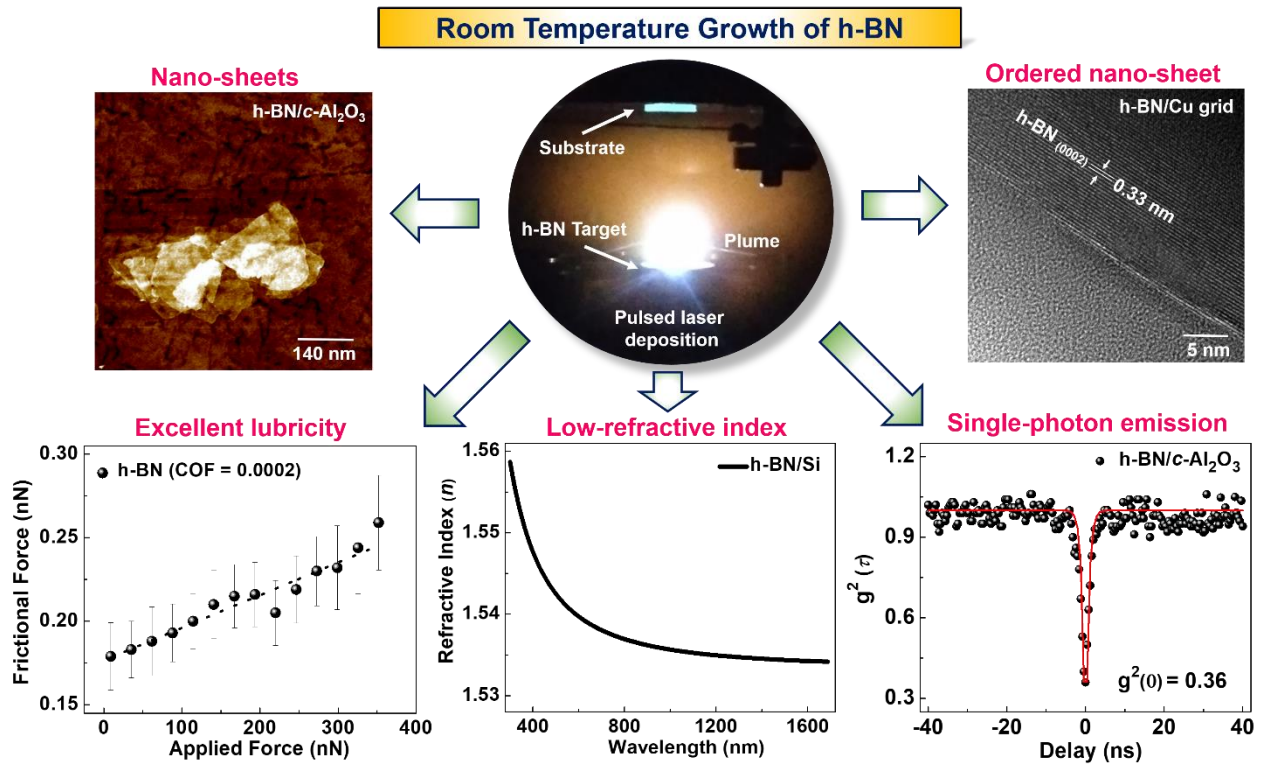
⁷Abhijit Biswas, Rishi Maiti and Frank Lee equally contributed to this work

*E-mail: abhijit.biswas@rice.edu, m.tripathi@sussex.ac.uk, a.gaeta@columbia.edu, ajayan@rice.edu

Keywords: h-BN; pulsed laser deposition; room-temperature growth; functional properties; quantum emission

Graphical abstract

Two-dimensional nanosheets-like hexagonal boron nitride (h-BN) are grown at room temperature by pulsed laser deposition (PLD) technique, exhibiting remarkable functional properties and application worthiness, thus creating a potential scenario for “*h-BN on demand*” under a frugal thermal budget, indispensable for nanotechnology.



Abstract

Room temperature growth of two-dimensional van der Waals (2D-vdW) materials is indispensable for state-of-the-art nanotechnology as it supersedes the requirement of elevated growth temperature accompanied with additional high thermal budgets, and the possibility of intrinsic interfacial thermal diffusion related deterioration of functional properties. Here, we demonstrated the growth of ultrawide-bandgap boron nitride (BN) at *room temperature* by using the pulsed laser deposition (PLD) process and demonstrated various functionalities for potential applications. Comprehensive chemical, spectroscopic and microscopic characterization confirms the growth of ordered nanosheets-like hexagonal BN (h-BN). Functionally, films show hydrophobicity, high lubricity (low coefficient of friction), low refractive index within the visible to near-infrared wavelength range, and room temperature single-photon quantum emission. Our work unveils an important step that brings a plethora of applications ranging from the precise design of photonic devices, quantum information technology, transparent lubricant coatings, chemically inert capping layers for corrosive and ambient-air degradable materials, and 2D flexible nano-electronics, thus creating a scenario for “*h-BN on demand*” at frugal thermal budget.

Two-dimensional van der Waals (2D-vdW) materials are astonishing in the nano-era, showing tremendous potential and technological relevance due to their unique atomic-scale growth, emergent functional properties, and application potentials (1,2). In general, several top-down (chemical and mechanical exfoliations) and bottom-up approaches (thin film growth by various physical/chemical vapor phase deposition techniques) have been employed to synthesize these 2D-vdW materials with atomic layer control (3-5). Among these, the liquid exfoliation methods produce large-area 2D-vdW materials, however, the film quality is found to be very low (due to the presence of adsorbates and surfactants on the surface). Whereas vapor-phase thin film growth processes lead to smaller size crystals, but with high crystalline quality (6). Due to this process-dependent variable quality, the growth of 2D-vdW materials thus remains to be an exceedingly intriguing research topic among the materials growth community. The formation, crystallinity, morphology, and consequent functional properties of 2D-vdW materials are highly sensitive to the thermodynamic and/or growth kinetics, adsorption of reaction species on a substrate surface, nucleation, and thus the resultant film growth and consequent properties (7,8).

Among various procedures, for large-scale growth, intrinsic property evaluation, and nano-device fabrications, chemical vapor deposition (CVD) has widely been adopted to grow the 2D-vdW materials (3,4). However, synthesizing 2D-vdW materials by CVD requires a very high-temperature of ~1000-1500 °C (sufficient supply of activation energy to adatoms to migrate to the energetically preferred locations onto the substrates during the growth); a rigorous synthesizing condition that limits device capabilities as elevated temperatures result in possible defect segregation and annihilation at the interfaces (9-12). Therefore, researchers are giving efforts to synthesize 2D-vdW materials at relatively lower-temperatures, with the trade-off in crystalline domain size/quality, but generating novel application possibilities (13-16). Theoretically, 2D material show anisotropy in growth and its kinetics can be controlled by adjusting the balance between elements (17). However, fundamentally, both thermodynamics (temperature) and kinetics play equally important roles, therefore temperature (i.e. ionized energetic species) during the vapor-phase deposition has always been critical, which also affects nucleation density and grain size (8,13). Therefore, the growth of 2D-vdW materials at lower or even at room temperature with a high-enough supply of kinetic energy directed towards reaction species might be sufficient to overcome the nucleation barrier, and if successful, would be very useful for several room-temperature applications. This would significantly enable the growth of 2D-vdW materials on any

given substrate (with varying degrees of crystallinity, thickness, and uniformity and consequent emergent phenomena), creating a scenario for “*thin films growth of 2D-vdW materials on demand*”, thereby ample investigations on properties and consequent applications.

To investigate this possibility of thin film *room-temperature* growth, we use hexagonal boron nitride (h-BN) as our model material. Among numerous 2D-vdW materials, ultra-wide bandgap h-BN (with a bandgap of ~ 5.9 eV) gets special attention for its excellent chemical inertness, high-thermal stability, and electronic, optical, and mechanical properties (**18,19**). Electronically, h-BN is suitable as a gate-dielectric layer for the 2D-based field effect transistors (FET) devices (**20**). Given these advantages, we attempt to grow h-BN thin films at room temperature by using a highly energetic and thermally non-equilibrium thin film growth process, pulsed laser deposition (PLD). PLD possesses several advantages over other growth methods, as it is not in thermal equilibrium, directed onto the substrate, and the stoichiometry is preserved throughout the thin film deposition process, starting from a dense crystalline target of the desired material (**21**). Several attempts have been implemented to grow h-BN films by PLD, however at elevated temperatures, showing mostly island-like growth (**22-27**). The plasma formation during the ablation process of the target by pulsed UV-laser (photon energy of ~ 5 eV) contains radicals and ions (e.g. B^+ , N^+ , N^* , N_2 , N_2^+ , N_2^{*+} and BN) of the ablated species with kinetic energy ~ 10 -100 eV (**Figs. 1a, 1b**) (**28**).

We have grown h-BN at room temperature on various substrates: *c*- Al_2O_3 (0001), holey Cu-grid, and Si (100) and investigated their growth characteristics and several functional properties. Chemical, morphological, spectroscopic, and electron microscopy characterizations confirm the growth of ordered h-BN nanosheets. We observed that films are hydrophobic, and exhibit a low-refractive index, and room temperature single-photon quantum emission. Moreover, the frictional characteristics reveal excellent lubrication properties with a low coefficient of friction. Thus, successful growth of ordered h-BN nanosheets by PLD at room temperature might usher in the growth of h-BN on a variety of substrates, generating ample potential application under reduced thermal budgets, e.g. for flexible 2D-electronics (**29**) coating layers for highly-corrosive materials, protecting layers for open-air degradable materials, precise photonic devices and for quantum information technology.

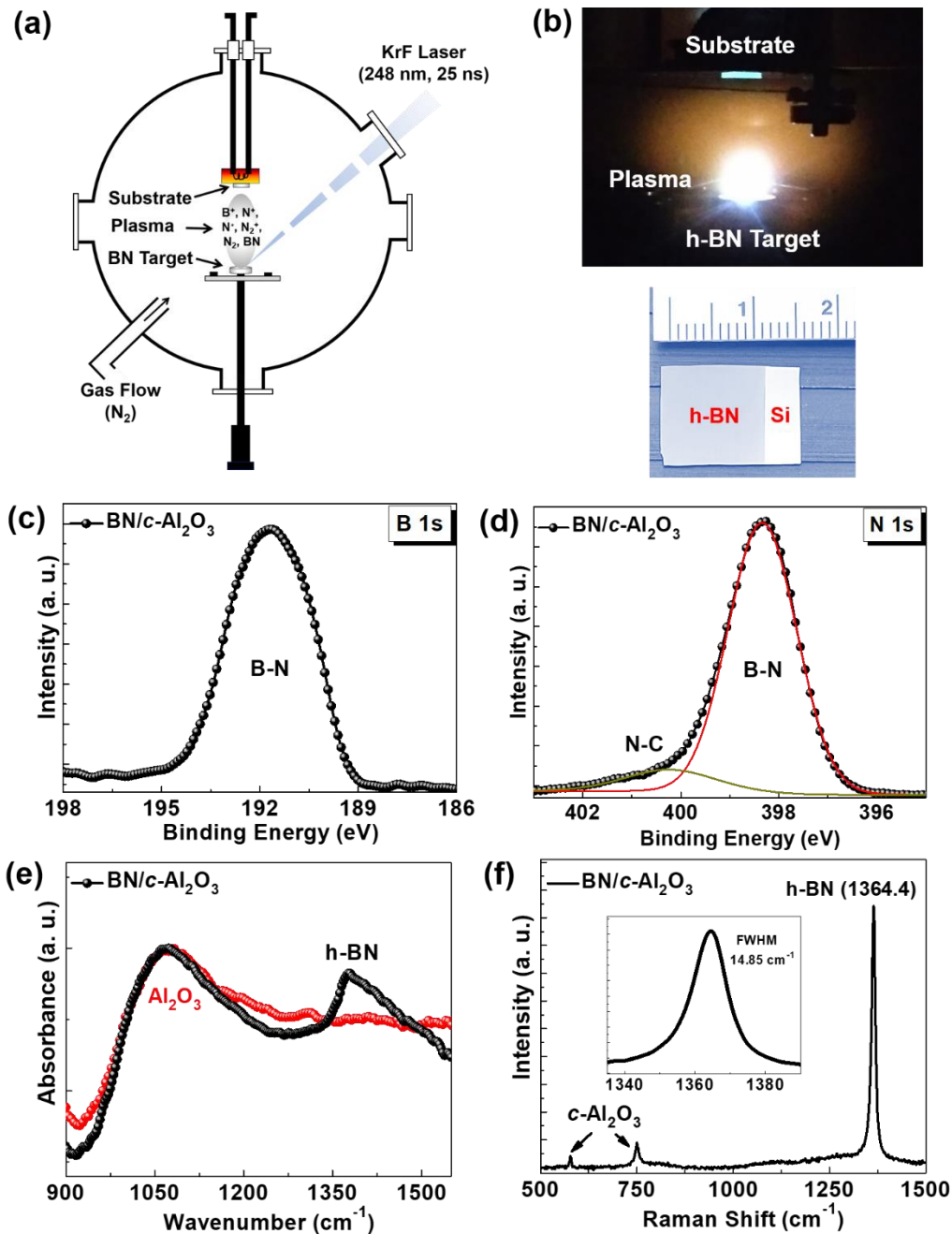


Fig. 1| Pulsed laser deposition of h-BN and its spectroscopic characterizations. (a) Schematic showing the thin film growth process by pulsed laser deposition. (b) Real-time plume generation (highly energetic) during the ablation of h-BN with ablated species deposited on a substrate kept at room temperature. An optical image of a uniform ($\sim 1 \times 1$ cm²) thick h-BN film (bottom). (c), (d) XPS elemental B 1s and N 1s core scans on c-Al₂O₃ confirm the presence of characteristics B-N bonds. (e), (f) FTIR and Raman spectra show the peak at ~ 1364 cm⁻¹, further confirming the growth of h-BN at room temperature.

Structurally, to characterize the grown h-BN films we first performed conventional B 1s and N 1s core-level X-ray photoelectron spectroscopy (XPS) elemental scans. Characteristically, we observed the B-N bonding-related peaks in both the elemental B 1s and N 1s core level scans with the π -plasmon peaks, characteristics of h-BN (**Figs. 1c, 1d**, and **Supplementary Information Figs. S1a and S1b**) (**30**). In N 1s scans, in addition to the B-N bonding peak, we observed a small shoulder of the N-C peak at ~ 400.5 eV (**Fig. 1d**), due to the ambient air exposure effect, related to adventitious carbon (**31**). Through valence band spectra (VBS), we observed the characteristic band structure of the h-BN film (two distinct features with maxima at ~ 12 and ~ 20 eV, corresponding to the overlapping of σ and π -band as well as s -band, respectively) with valence band maxima (VBM) position at ~ 1.7 eV (**Supplementary Information Fig. S1c**) (**32,33**). In order to confirm the phase, we then performed Fourier transformed infrared (FTIR) spectroscopy and Raman spectroscopy. FTIR shows a peak within $1350\text{-}1500\text{ cm}^{-1}$, attributed to the in-plane B-N stretching vibrations (transverse optical mode) of the sp^2 -bonded h-BN (**Fig. 1e**) (**34**). Moreover, in Raman spectra we observed Raman-active in-plane E_{2g} phonon mode at $\sim 1364\text{ cm}^{-1}$ (**Fig. 1f**), (**30**) with a narrow full-width at half maxima (FWHM) of $\sim 14.85\text{ cm}^{-1}$. All these spectroscopic characterizations evince the room-temperature growth of h-BN.

Hereafter, we investigated the surface morphology of film by using atomic force microscopy (AFM). Interestingly, it shows 2D nanosheets-like morphology (on $c\text{-Al}_2\text{O}_3$) (**Fig. 2a**). The lateral sizes of these h-BN sheets are $\sim 200\text{-}300$ nm. Furthermore, to confirm the crystalline nature, we performed top-view high-resolution transmission electron microscopy (HRTEM) by growing h-BN films directly on holey Cu grid. For HRTEM, we have grown ultra-thin BN films by providing only few numbers of laser shots (100 laser shots to be precise). As seen from the HRTEM (**Fig. 2b**), we also observed the nano-crystal-like feature. Remarkably, a closer inspection shows the appearance of clear ordered lattice fringes (**Fig. 2c**), which were further processed using an Inverse Fast Fourier Transform (IFFT) to measure the actual inter-planar distance (d) which was found to be ~ 0.33 nm (**Fig. 2d**), corresponds to the (0002) plane of h-BN (**18,19**). This establishes the growth of ordered nanosheets-like h-BN at room temperature.

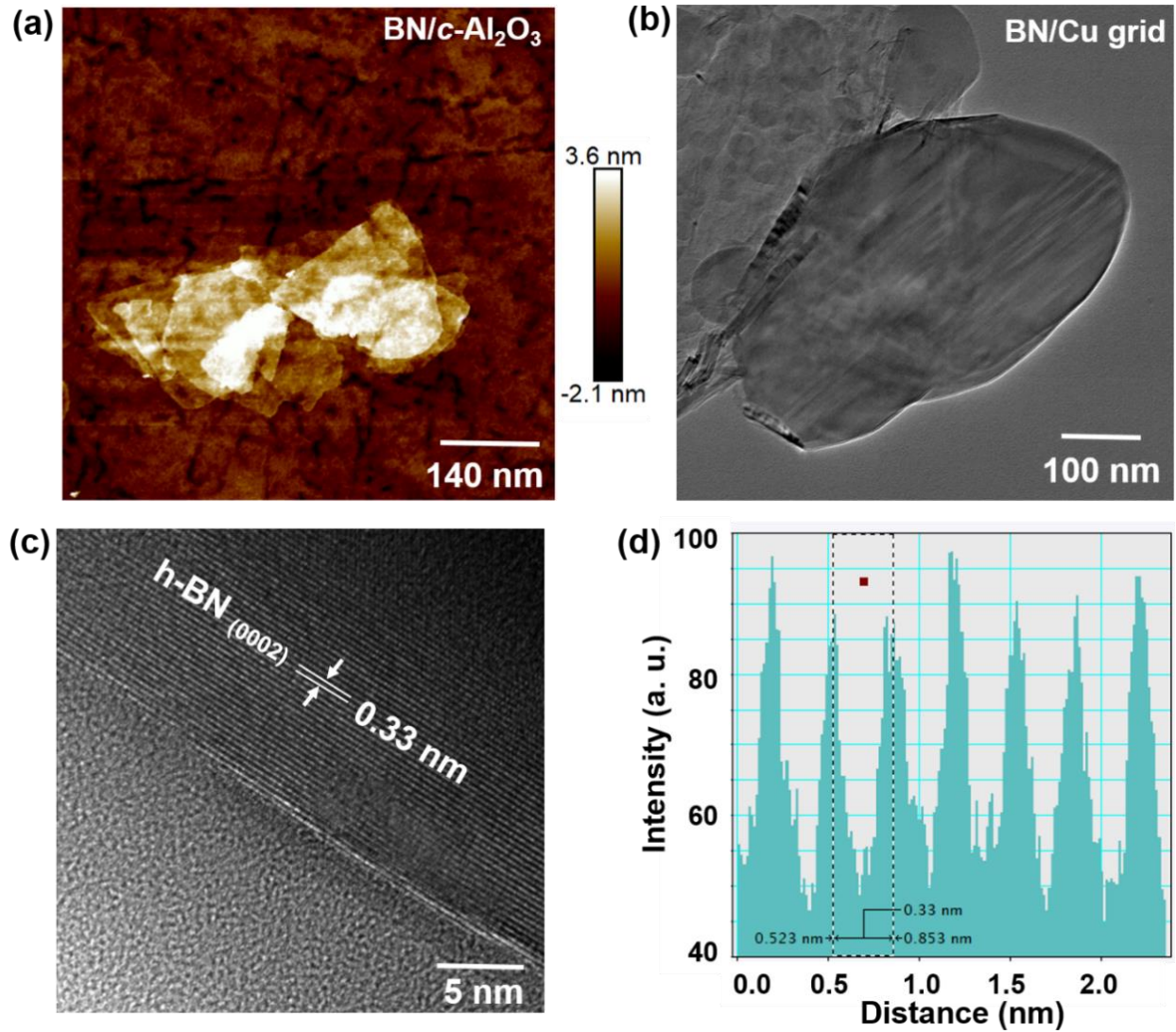


Fig. 2| Microscopic characterizations of h-BN. (a) AFM topography shows the nanosheets-like growth. (b), (c) High-resolution transmission electron microscopy (HRTEM) also shows the sheet-like structure. (d) Inter-planar d spacing of ~ 0.33 nm, corresponding to the (0002) lattice plane of h-BN. For HRTEM, a few shots of BN was supplied directly on the holey Cu grid.

As mentioned earlier, the room temperature growth of highly ordered nanosheets is extremely interesting and cost-effective for scale-up, as it can be grown on potentially any given substrate (e.g. foils, flexible polymer surfaces), widening the horizon of h-BN growth for applications (18). There have been attempts to grow BN at room temperature by RF sputtering and atomic layer depositions (ALD), but have come up with an amorphous/turbostratic phase

(35,36). In the case of PLD, which is most often used for metal-oxides thin film depositions, it is well known that high-temperature (≥ 700 °C) is needed for epitaxial growth (depending on the thermodynamics) (21). However, as reported by Elhamid *et al.*, well-defined graphene can be grown at room temperature by PLD on a bi-metallic Ni-Cu substrate, where laser power played a crucial role, favoring nucleation activation energy which promotes graphene formation (37). Rasic *et al.* grew metallic TiN thin films on sapphire at room-temperature (38). Kakehi *et al.* reported the epitaxial growth of NiO (111) thin films by PLD at room-temperature (39). Ma *et al.* grew ZnO films on glass at room temperature by PLD (40). Fundamentally, adsorption energy is one order higher than the diffusion energy barrier and at lower temperature, the adsorption rate exceeds the desorption rate (13). Therefore, small-fractal shaped domain growth has been observed for vapor-phase synthesis for 2D materials at high flux and at reduced temperature (13). Hence, from growth perspective, an energetic bombardment of particles during the growth process is necessary to synthesize BN film at lower/room temperature, with the ability for the adatoms to overcome the substrate diffusion energy barrier. Considering PLD is a highly energetic deposition process and in addition BN contains light elements, thus synergistically, created vapor pressure and kinetic energy of the laser-ablated species in the plasma form possibly sufficient to migrate to the substrate and nucleate onto it (within a few μ S) and forms the films even at room temperature, affecting the nucleation density and grain size (13,21), at least for the present employed growth protocols.

To realize the intrinsic functional properties of the h-BN film, first, we investigate the wetting characteristics by the contact angle (CA) measurement, as hydrophobic surfaces are known as effective protective layers in harsh environments with extreme temperatures, and h-BN provides strong resistance to chemical attack and high-temperature stability (17). As observed, h-BN tends toward minimizing the contact surface with water. Films exhibit hydrophobic behavior which is fairly increased by $\sim 5\%$, (CA: $55^\circ \pm 1$ to $60^\circ \pm 1$) (Fig. 3a), consistent with the fact of the polar character of the boron-nitrogen bond ($-N^{\ominus}B^{\oplus}-$), as the wettability is strongly influenced by the vdW interactions (41). The measured CA is also in agreement with the reported values ranging between ~ 50 - 67° (41). Fundamentally, the wetting characteristics of a particular material also depend on the surface roughness and are inherent to the wetting phenomena (42,43). However, considering that the surface roughness of grown h-BN film is of few nm (~ 2 - 3 nm); the effect of roughness on the CA may be insignificant here.

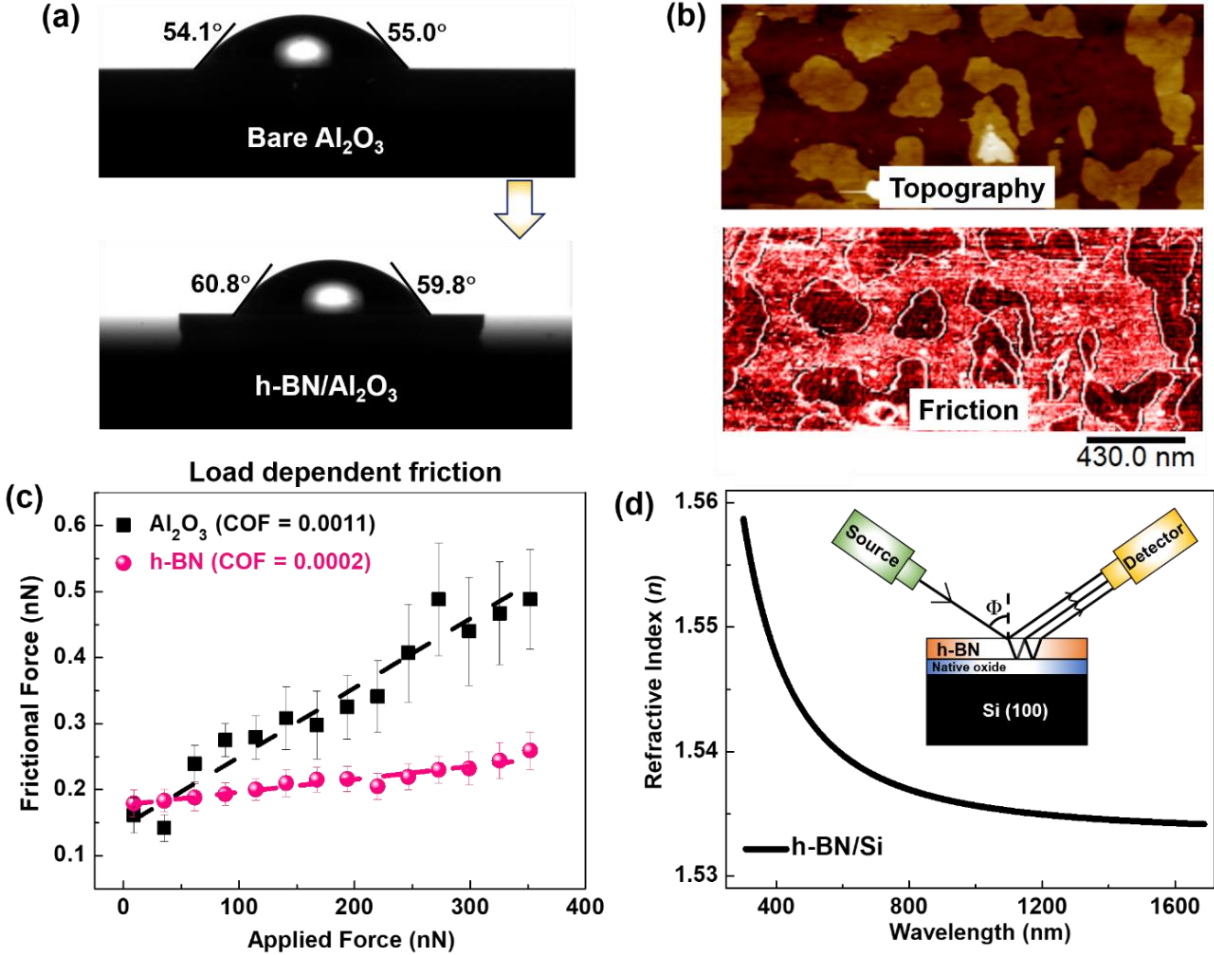


Fig. 3| Functional properties of h-BN. (a) Contact angle measurement on the h-BN surface, showing the water repelling nature. (b) Topography (upper panel) and the corresponding frictional force (lower panel) map of h-BN/ $c\text{-Al}_2\text{O}_3$. Darker colors in the frictional force map at the h-BN suggest lower friction. (c) The measured frictional force with different loading. The slope of the fitted line represents the coefficient of friction (COF) of the material. (d) The refractive index (n) of the h-BN film (grown on Si substrate). The inset shows the schematic of the measurement.

At the submicron scale, the intrinsic roughness and moderately hydrophobic surface influence the tribological response. Thus, the frictional characteristics of h-BN (on $c\text{-Al}_2\text{O}_3$) are examined by lateral force microscopy where the topography and the corresponding frictional force map are measured at the same acquisition (**Fig. 3b**). The presence of h-BN layers anticipates lower friction force values than the surrounded $c\text{-Al}_2\text{O}_3$ substrate. However, the edges and step-edges lead to the highest friction values due to the higher susceptibility of edge atoms towards the slider (tip apex)

which is peculiar to the family of 2D-vdW materials (**44,45**). The tendency of the lubrication is further monitored where the same region of h-BN and *c*-Al₂O₃ are swept by the probe with increasing applied normal force ranging from 10 nN to 350 nN (**Fig. 3c**). We observed a linear response of increase in friction force as the function of normal forces, where the trend of load-dependent friction is higher for the alumina substrate as compared to the h-BN, quantified through linear fit resulting in the coefficient of friction (COF). The COF values of h-BN and *c*-Al₂O₃ are obtained as ~0.0002 and ~0.0011, respectively. It is noteworthy that COF is an extrinsic property, which depends on the local contact area at the interface. The present study comprises a miniature surface area AFM tip (radius \approx 10 nm) leading to the smaller value of COF. Nevertheless, the ratio of the COF and frictional properties are comparable to the conventionally fabricated h-BN sheets (**46,47**). The frictional force values decrease systematically with the increasing number of h-BN layers (\sim 3-10 nm) due to mitigation of the “puckering” effect (**44**), in front of the sliding tip apex (Supplementary Information **Fig. S2**). Overall, the observed hydrophobic nature and lubricity properties of h-BN would be useful for the coating industry.

Furthermore, we measured the refractive index (*n*) of an h-BN film grown on Si substrate (see Supplementary Information **Fig. S3** for the details characterizations of the film), which was found to be ~1.53-1.55 (**Fig. 3d**) within the visible and near-infrared spectral range. We used variable angle spectroscopic ellipsometry (VASE) to measure the refractive index (*n*). The schematic of the measurement is depicted in the inset of **Fig. 3d**. Considering the nanosheets-like morphology of h-BN, thus we fitted the ellipsometry data by applying the Bruggeman effective-media approximation (EMA) method that considers the film as h-BN with defects (See method section and Supplementary Information **Fig. S4**). Interestingly, the h-BN with added voids into the fitting model provides lower *n* than the perfect single crystalline layer h-BN fitting (*n* \sim 1.8). The lower *n* is adequate as stoichiometry, porosity, roughness affects the value of *n* (**48,49**). Interestingly, the lower *n* is helpful for the precise designing of photonic devices operating in visible and near-infrared wavelengths range (**48**).

Since nanosheets-like h-BN can host defects such as point defect including boron-vacancy (V_B) and/or nitrogen-vacancy (V_N), paramagnetic center from negatively charged boron (V_B^-) or nitrogen vacancies (V_N^-), and nitrogen-vacancy and boron replaces nitrogen ($V_N N_B$), thus it may show single photon emission (SPE) at room temperature, attributed to these localized defects states

inside the bandgap (**50-53**). SPE in h-BN is extremely important for the next-generation quantum computing and information-processing technologies, considering its excellent chemical and thermal robustness (**54,55**). **Figure 4a** shows confocal photoluminescence (PL) map ($\sim 50 \times 50 \mu\text{m}^2$) of h-BN nanosheets showing much brighter emission spots (yellow) above the background. **Figure 4b** shows the corresponding PL emission spectrum under continuous wave non-resonant excitation ($\lambda = 532 \text{ nm}$). The emitter has a sharp zero-phonon line (ZPL) at $\sim 577 \text{ nm}$ with an asymmetric shape (FWHM $\sim 2 \text{ nm}$), extracted from a single Lorentzian fit. A weak optical phonon replica is visible around $\sim 630 \text{ nm}$, red-shifted by $\geq 165 \text{ nm}$ from the ZPL peak, related to phonon sidebands (PSB) (**56**). It should be noted that the small peak at $\sim 580 \text{ nm}$ is most likely a ZPL of another weak emitter within the excitation spot. In order to understand the extent of the electron-phonon coupling we calculate the Debye-Waller factor (the ratio between ZPL intensity to the total emission) is found to be ~ 0.70 .

In order to understand the polarization behavior of the localized emission, we performed emission polarization measurements. **Figure 4c** corresponds to the angular diagram of emission, which reflects a well-defined dipole-like character for the single isolated defect. The corresponding fits are obtained using a $\cos^2(\theta)$ fitting function, which yields an emission polarization visibility of $\sim 75\%$, suggesting a single dipole transition linearly oriented along the basal plane of the h-BN nanocrystals. **Figure 4d** displays the second-order correlation function $g^2(\tau)$ using two Si APDs, mounted in a Hanbury-Brown and Twiss (HBT) configuration to establish the quantum nature of the emitted light from the defects of h-BN nanocrystals. The $g^2(0)$ is found to be ~ 0.36 , well below of 0.5 (without background correction) at zero delay time (**Fig. 4d**), which clearly indicates the anti-bunching of the emission (**54**). The experimental $g^2(\tau)$ data can be fitted well with the three-level model: $g^2(\tau) = 1 - (1+a)e^{-|\tau|/\tau_1} + ae^{-|\tau|/\tau_2}$, where a is a fitting parameter, τ_1 and τ_2 are the lifetimes of the excited and metastable states, respectively. Moreover, the radiative lifetime $\tau_1 \sim 3 \text{ ns}$ is consistent with that of the previous report (**56**). However the non-radiative lifetime τ_2 is much longer. These observations clearly show the room temperature stable SPE in h-BN. Our results indicate this stable and bright SPE observed in the visible range at room temperature potentially could solve the long-term issues of the on-chip integration of deterministic SPEs over large scales. Our approach of growing h-BN nanosheets even at room temperature depicts the ability to directly grow 2D layers onto designed electronic/photonic structures, which can be very useful for

integrated circuits applications since it avoids any chemical contaminants or material deformation that often occurs with the wet or dry transfer.

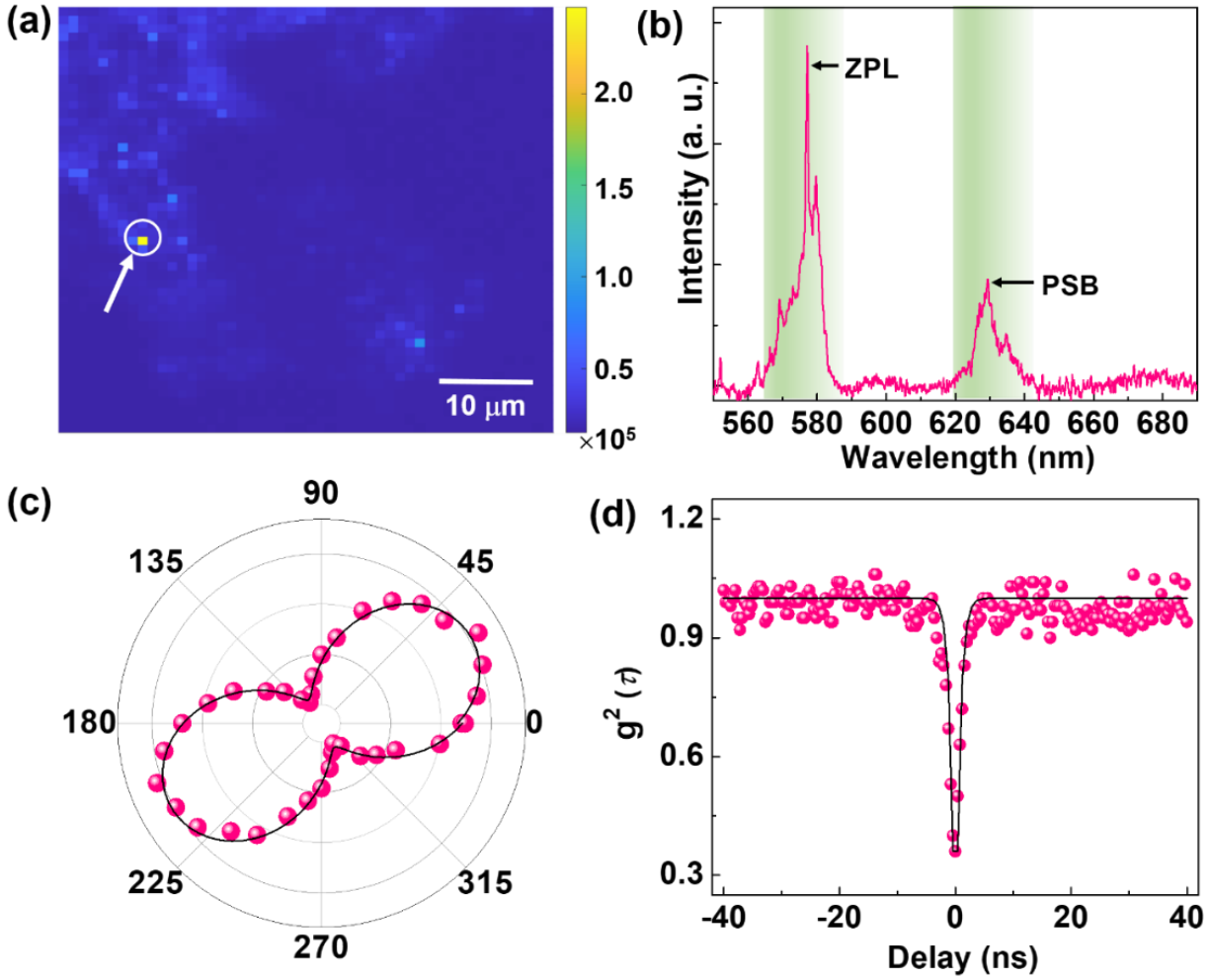


Fig. 4| Room-temperature photo-physical properties of h-BN nanosheets. (a) Confocal photoluminescence map ($\sim 50 \times 50 \mu\text{m}^2$) corresponds to the ultra-bright (yellow spots) defect-assisted emission from h-BN nanosheets grown on sapphire. (b) Photoluminescence spectrum under 532-nm laser excitation and a 550-nm long-pass filter at room temperature. (c) The emission (red spheres) polarization curve. The red curve is fitted using a $\cos^2\theta$ function indicating an atomic defect with the in-plane dipole moment. (d) Second-order autocorrelation measurement $g^{(2)}(\tau)$ of the defect with a dip at $g^{(2)}(0) \approx 0.36$, suggesting the antibunching nature of light.

In summary, we have grown ordered nanosheets of h-BN, by PLD at room temperature. Extensive characterizations confirm the growth of h-BN sheets with improved-hydrophobicity, low refractive index in the visible wavelength range, and room temperature single-photon quantum emission. Furthermore, h-BN layers show excellent lubricity with a reduction in the friction force coefficient than that of the subsurface. Our observation of room-temperature growth of h-BN exhibiting astonishing functional properties indicates that it could be grown on any substrate (e.g. on metals, foils, and flexible polymers). Furthermore, optical characterizations of the grown h-BN nanosheets show immense potential for several applications, such as in the precise design of photonic devices, quantum sensing and detection, transparent coating, and capping/protective layers for degradable materials, thus possibly creating a scenario for “*h-BN on demand*”.

Experimental Methods

Thin film growth (Pulsed Laser Deposition). BN films were grown by PLD (KrF excimer laser with operating wavelength of 248 nm, and pulse width of 25 ns). Films were grown at room-temperature by using the following deposition conditions: laser fluency $\sim 2.2 \text{ J/cm}^2$ (laser energy $\sim 230 \text{ mJ}$), repetition rate 5 Hz, high-purity (5N) nitrogen gas partial pressure (P_{N_2}) $\sim 100 \text{ mTorr}$ (flow rate $\sim 73 \text{ sccm}$), and target to substrate distance $\sim 50 \text{ mm}$. We used commercially available high-purity (99.9% metal basis) polycrystalline h-BN target for the ablation (American Element). For substrates, we used hexagonal $c\text{-Al}_2\text{O}_3$ (0001), Si (100), and holey Cu grid as substrates with 2000 laser pulses (on Al_2O_3), 5000 laser pulses (on Si) and 100 laser pulses (on holey Cu grid) was given to the target, respectively.

Chemical and microscopic characterizations (XPS, VBS, FTIR, AFM, Raman, and HRTEM). X-ray photoelectron spectroscopy was performed with a PHI Quantera SXM scanning X-ray microprobe with 1486.6 eV monochromatic Al K_α X-ray source. FTIR was obtained by using the Nicolet 380 FTIR spectrometer, equipped with a single-crystal diamond window. Park NX20 AFM was used to obtain surface topography, operating in tapping mode using Al-coated Multi75Al cantilevers. Raman spectroscopy was performed using a Renishaw inVia confocal microscope, with a 532 nm laser as the excitation source. For HRTEM, the ultra-thin film was grown on holey Cu-grid and the images were recorded using Titan Themis operating at 300 kV.

Adhesion and friction force characterizations. Atomic force microscopy (from Bruker Ltd.) was operated in Bruker ScanAsyst using peak force tapping mode (Bruker's proprietary) with an applied normal force of 1 nN. All the AFM operations were carried out at room temperature under $\sim 35\text{-}40\%$ of relative humidity. Silicon nitride cantilever (stiffness $\sim 0.8 \pm 0.15 \text{ N/m}$) was used for the topography measurements. The friction force (nN) was measured in the mode of "lateral force microscopy", here silicon cantilever of stiffness (0.4 N/m by Sader's method has been used for the investigations (57)). The average values of lateral force in trace and retrace direction are measured as half times of trace minus retrace (TMR). This procedure is useful to mitigate the topographical

effect in the friction measurements. The tip radii are evaluated through the blind tip reconstruction technique using a grating sample as described in previous studies (58).

Optical characterizations (Refractive index and single-photon emission). Variable angle spectroscopic ellipsometry (VASE) (M-2000 Ellipsometer by J. A. Woollam Company) was applied to measure the refractive index (RI). The RI of a bare silicon substrate with a thin native oxide layer on the top is measured first as a reference, followed by the RI of the film. Two sequential measurements followed a similar process. Incidents of four different angles equally spaced from $\Phi = 55^\circ$ to 70° were sequentially shed on the surface of the samples that were placed on a horizontal stage and the corresponding reflected light was collected by a detector. The original spectroscopic data were then fitted using two types of three-layer models (see the **Supplementary Information Figure S4** for their detailed comparison).

In both models, a two-layer reference model that consists of a pure silicon substrate beneath a 1.72 nm native oxide layer was applied to represent the silicon substrate. Then a third layer was added on top of the reference model to represent the grown h-BN film. We used a Bruggeman effective-media approximation (EMA) layer that mixes the pure h-BN with voids ($n=1$). The light spot generated by the ellipsometer has a diameter at a scale of hundreds of microns, which is large enough to bring an average effect for the BN film. We also used the pure h-BN part as the third layer. The fitting result of this model gave an unacceptable MSE greater than 600, not a suitable fitting parameter.

We performed single photon emission at room temperature by using a conventional confocal, optical microscope and a Hanbury-Brown and Twiss (HBT) interferometer. The emitted light is collected by an air objective (100x, NA 0.95) and detected by using avalanche photodiodes or a spectrometer. A 532 nm CW laser diode was used to excite the SPEs. A dichroic mirror (cutoff wavelength 532 nm) and a long pass filter (cutoff wavelength 550 nm) allowed suppressing the back-reflected pump beam. The signal was fiber-coupled to either a grating spectrometer (Ocean optics, QE65pro) or avalanche photodiodes (Excelitas) with 30% collection efficiency in the relevant wavelength range, and the detection event was recorded using a time-tagged single photon-counting module (TTM8000).

Supplementary Information

The online version contains supplementary material available at <https://doi.org/>.

Acknowledgements

This work was sponsored by the Army Research Office and was accomplished under Cooperative Agreement Number W911NF-19-2-0269. The views and conclusions contained in this document are those of the authors and should not be interpreted as representing the official policies, either expressed or implied, of the Army Research Office or the U.S. Government. The U.S. Government is authorized to reproduce and distribute reprints for Government purposes notwithstanding any copyright notation herein. T. Li and Y. Zhao are supported as part of ULTRA, an Energy Frontier Research Center funded by the US Department of Energy (DOE), Office of Science, Basic Energy Sciences (BES), under Award No. DE-SC0021230. Manoj Tripathi and Alan Dalton would like to thank strategic development funding from the University of Sussex.

Author contributions

A. B., R. V. & P. M. A. conceptualized the study. A.B., A. B. P., S. A. I., C. L., H. K., X. Z., T. G., M. S. R. S. & J. L. grew and characterized the films. F. L., M. T. & A. D. did the adhesion and friction force characterizations. T. L. & Y. Z. carried out the refractive index measurement. R. M., C. Y. C. & A. L. G. conducted the single photon emission experiment. A. G. B., M. R. N., D. A. R., P. B. S. & T. I. commented on the manuscript. All the authors discussed the results and contributed on the manuscript preparation.

Conflict of Interest

The authors declare no conflict of interest.

Data availability

The data that support the findings of this study are available from the corresponding authors upon reasonable request.

References

1. Das, S., Robinson, J. A., Dubey, M., Terrones, H. & Terrones, M. **Beyond Graphene: Progress in Novel Two-Dimensional Materials and van der Waals Solids**, *Ann. Rev. Mat. Res.* **45**, 1-27 (2015).
2. Xu, X., Guo, T., Kim, H., Hota, M. K., Alsaadi, R. S., Lanza, M., Zhang, X. & Alshareef, H. N. **Growth of 2D Materials at the Wafer Scale**, *Adv. Mater.* **34**, 2108258 (2021).
3. Zhang, Y., Yao, Y., Sendeku, M. G., Yin, L., Zhan, X., Wang, F., Wang, Z. & He, H. **Recent Progress in CVD Growth of 2D Transition Metal Dichalcogenides and Related Heterostructures**, *Adv. Mater.* **31**, 1901694 (2019).
4. Cai, Z., Liu, B., Cheng, H. M. & Naguib, M. **Chemical Vapor Deposition Growth and Applications of Two-Dimensional Materials and Their Heterostructures**, *Chem. Rev.* **118**, 13, 6091–6133 (2018).
5. Huo, C., Yan, Z., Song, X. & Zeng, H. **2D materials via liquid exfoliation: a review on fabrication and applications**, *Science Bulletin*, **60**, 1994 (2015).
6. Tong, X., Liu, K., Zeng, M. & Fu, L. **Vapor-phase growth of high-quality wafer-scale two-dimensional materials**, *InfoMat* **1**, 460-478 (2019).
7. Dong, J., Zhang, L., Dai, X. & Ding, F. **The epitaxy of 2D materials growth**, *Nat. Commun.* **11**, 5862 (2020).
8. Dong, J., Zhang, L. & Ding, F. **Kinetics of Graphene and 2D Materials Growth**, *Adv. Mater.* **31**, 1801583 (2018).
9. Zhu, Z., Zhan, S., Zhang, J., Jiang, G., Yi, M., & Wen, J. **Influence of growth temperature on MoS₂ synthesis by chemical vapor deposition**, *Mater. Res. Express* **6**, 095011 (2019).
10. Yamada, H., Inotsume, S., Kumagai, N., Yamada, T. & Shimizu, M. **Growth Temperature Effects of Chemical Vapor Deposition-Grown Boron Nitride Layer Using B₂H₆ and NH₃**, *physica status solidi (b)*, **257**, 1900521 (2019).
11. Chen, Y., Liang, H., Xia, X., Zhang, H., Shi, J., Abbas, Q. & Du, G. **Growth temperature impact on film quality of hBN grown on Al₂O₃ using non-catalyzed borazane CVD**, *J Mater Sci: Mater Electron*, **28**, 14341 (2017).
12. S. H. Lee, H. Jeong, O. F. N. Okello, S. Xiao, S. Moon, D. Y. Kim, G.-Y. Kim, J. -I. Lo, Y. -C. Peng, B. -M. Cheng, H. Miyake, S.-Y. Choi, J. K. Kim, **Improvements in**

- structural and optical properties of wafer-scale hexagonal boron nitride film by post-growth annealing**, *Sci. Rep.* **9**, 10590 (2019).
13. Kozhakhmetov, A., Torsi, R., Chen, C. Y. & Robinson, J. A. **Scalable low-temperature synthesis of two-dimensional materials beyond graphene**, *J. Phys. Mater.* **4**, 012001 (2020).
 14. Mun, J., Kim, Y., Kang, I. S., Lim, S. K., Lee, S. J., Kim, J. W., Park, H. M., Kim, T., & Kang, S. -W. **Low-temperature growth of layered molybdenum disulphide with controlled clusters**, *Sci. Rep.* **6**, 21854 (2016).
 15. Ahn, C., Lee, J., Kim, H., Bark, H., Jeon, M., Ryu, G. H., Lee, Z., Yeom, G. Y., Kim, K., Jung, J., Kim, Y., Lee, C. & Kim, T. **Low-Temperature Synthesis of Large-Scale Molybdenum Disulfide Thin Films Directly on a Plastic Substrate Using Plasma-Enhanced Chemical Vapor Deposition**, *Adv. Mater.* **27**, 5223 (2015).
 16. Zhao, Y., Song, J. G., Ryu, G. H., Ko, K. Y., Woo, W. J., Kim, Y., Kim, D., Lim, J. H., Lee, S., Lee, Z., Park, J. & Kim, H. **Low-temperature synthesis of 2D MoS₂ on a plastic substrate for a flexible gas sensor**, *Nanoscale*, **10**, 9338 (2018).
 17. Zhang, Z., Liu, Y., Yang, Y. & Yakobson, B. I. **Growth Mechanism and Morphology of Hexagonal Boron Nitride**, *Nano Lett.* **16**, 2, 1398–1403 (2016).
 18. Zhang, K., Feng, Y., Wang, F., Yang, Z. & Wang, J. **Two dimensional hexagonal boron nitride (2D-hBN): synthesis, properties and applications**, *J. Mater. Chem. C*, **5**, 11992-12022 (2017).
 19. Roy, S., Zhang, X., Puthirath, A. B., Meiyazhagan, A., Bhattacharyya, S., Rahman, M. M., Babu, G., Susarla, S., Saju, S. K., Tran, M. K., Sassi, L. M., Saadi. M., Lai, J., Sahin, O., Sajadi, S. M., Dharmarajan, B., Salpekar, D. & Chakingal, N. et al. **Structure, Properties and Applications of Two-Dimensional Hexagonal Boron Nitride**, *Adv. Mater.* **33**, 2101589 (2021).
 20. Dean, C. R., Young, A. F., Meric, I., Lee, C., Wang, L., Sorgenfrei, S., Watanabe, K., Taniguchi, T., Kim, P., Shepard, K. L. & Hone, J. **Boron nitride substrates for high-quality graphene electronics**, *Nat. Nano.* **5**, 722-726 (2010).
 21. Aziz, M. J. **Film growth mechanisms in pulsed laser deposition**, *Appl. Phys. A* **93**, 579-587 (2008).

22. Glavin, N. R., Jespersen, M. L., Check, M. H., Hu, J., Hilton, A. M., Fisher, T. S. & Voevodin, A. A. **Synthesis of few-layer, large area hexagonal-boron nitride by pulsed laser deposition**, *Thin Solid Films* **572**, 245 (2014).
23. Yang, Z. & J. Hao, J. **Progress in pulsed laser deposited two dimensional layered materials for device applications**, *J. Mater. Chem. C* **4**, 8859 (2016).
24. Velazquez. D., Seibert, R., Man, H., Spentzouris, L. & Terry, J. **Pulsed laser deposition of single layer, hexagonal boron nitride (white graphene, h-BN) on fiber-oriented Ag(111)/SrTiO₃(001)**, *J. Appl. Phys.* **119**, 095306 (2016).
25. Narayan, J., Bhaumik, A. & Xu, W. **Direct conversion of h-BN into c-BN and formation of epitaxial c-BN/diamond heterostructures**, *J. Appl. Phys.* **119**, 185302 (2016).
26. Wang, G., Chen, J., Meng, J., Yin, Z., Jiang, J., Tian, Y., Li, J., Wu, J., Jin, P. & Zhang, X. **Direct growth of hexagonal boron nitride films on dielectric sapphire substrates by pulsed laser deposition for optoelectronic applications**, *Fundamental Research* **1**, 677–683 (2021).
27. Acacia, N., Fazio, E., Neri, F., Ossi, P. M., Trusso, S. & N. Santo, N. **Pulsed laser deposition of boron nitride thin films**, *Radiat. Eff. Defects Solids: Incorporating Plasma Science and Plasma Technology* **163**, 293 (2008).
28. Glavin, N. R., Muratore, C., Jespersen, M. L., Hu, J., Fisher, T. S. & Voevodin, A. A. **Temporally and spatially resolved plasma spectroscopy in pulsed laser deposition of ultra-thin boron nitride films**, *J. Appl. Phys.* **117**, 165305 (2015).
29. Akinwande, D., Petrone, N. & Hone, J. **Two-dimensional flexible nanoelectronics**, *Nat. Commun.* **5**, 5678 (2014).
30. Saha, S., Rice, A., Ghosh, A., Hasan, S. N. M., You, W., Ma, T., Hunter, A., Bissell, L. J., Bedford, R., Crawford, M. & Arafin, S. **Comprehensive characterization and analysis of hexagonal boron nitride on sapphire**, *AIP Advances* **11**, 055008 (2021).
31. Shen, T., Liu, S., Yan, W. & Wang, J. **Highly efficient preparation of hexagonal boron nitride by direct microwave heating for dye removal**, *J. Mater. Sci.* **54**, 8852 (2019).
32. Widmayer, P., Boyen, H. G., Ziemann, P., Reinke, P., Oelhafen, P. **Electron spectroscopy on boron nitride thin films: Comparison of near-surface to bulk electronic properties**, *Phys. Rev. B* **59**, 5233 (1999).

33. Zhi, C., Ueda, S., Zeng, H., Wang, X., Tian, W., Wang, X., Bando, Y. & Golberg, D. **Weak morphology dependent valence band structure of boron nitride**, *J. Appl. Phys.* **114**, 054306 (2013).
34. Singh, R., Kalita, G., Mahyavanshi, R. D., Adhikari, S., Uchida, H., Tanemura, M., Umeno, M. & Kawahara, T. **Low temperature wafer-scale synthesis of hexagonal boron nitride by microwave assisted surface wave plasma chemical vapour deposition**, *AIP Adv.* **9**, 035043 (2019).
35. Abbas, Q., Liang, H., Shi, J., Chen, Y., Xia, X., Ahmad, A., Liu, J. & Du, G. **Growth and characterization of amorphous boron nitride dielectric films on Si via RF sputtering at room temperature**, *Mater. Lett.* **227**, 284 (2018).
36. Sprenger, J. K., Sun, H., Cavanagh, A. S., Roshko, A., Blanchard, P. T. & George, S. M. **Electron-Enhanced Atomic Layer Deposition of Boron Nitride Thin Films at Room Temperature and 100 °C**, *J. Phys. Chem. C* **122**, 17, 9455 (2018).
37. Abd Elhamid, A. M., Aboulfotouh, A. M., Hafez, M. A. & Azzouza, I. M., **Room temperature graphene growth on complex metal matrix by PLD**, *Diamond and Related Materials* **80**, 162 (2019).
38. Rasic, D., Sachan, R., Chisholm, M. F., Prater, J. & Narayan, J. **Room Temperature Growth of Epitaxial Titanium Nitride Films by Pulsed Laser Deposition**, *Cryst. Growth Des.* **17**, 6634 (2017).
39. Kakehi, Y., Nakao, S., Satoh, K. & Kusaka, T. **Room-temperature epitaxial growth of NiO(1 1 1) thin films by pulsed laser deposition**, *J. Cryst. Growth* **237**, 591 (2002).
40. Ma, X., Zhang, J., Lu, J. & Ye, Z. **Room temperature growth and properties of ZnO films by pulsed laser deposition**, *Appl. Surf. Sci.* **257**, 1310 (2010).
41. Boinovich, L. B., Emelyanenko, A. M., Pashinin, A. S., Lee, C. H., Drelich, J. & Yap, Y. K. **Origins of Thermodynamically Stable Superhydrophobicity of Boron Nitride Nanotubes Coatings**, *Langmuir* **28**, 1206 (2012).
42. Annamalaia, M., Gopinadhan, K., Han, S. A., Saha, S., Park, H. J., Cho, E. B., Kumar, B., Kim, S. -W. & T. Venkatesan, T. **On the nature of wettability of van der Waals heterostructures**, *Nanoscale* **8**, 5764 (2016).

43. Snapp, P., Kim, J. M., Cho, C., Leem, J., Haque, M. F. & Nam, S.W. **Interaction of 2D materials with liquids: wettability, electrochemical properties, friction, and emerging directions**, *NPG Asia Materials* **12**, 22 (2020).
44. Tripathi, M., Mahmood, H., Novel, D., Iacob, E., Vanzetti, L., Bartali, R., Speranza, G., Pegoretti, A. & Pugno, N. **Nanoscale friction of graphene oxide over glass-fibre and polystyrene**, *Composites Part B: Engineering* **148**, 272-280 (2018).
45. Tripathi, M., Awaja, F., Bizao, R. A., Signetti, S., Iacob, E., Paolicelli, G., Valeri, S., Dalton, A. & Pugno, N. M. **Friction and Adhesion of Different Structural Defects of Graphene**, *ACS Appl. Mater. Interfaces* **10**, 44614 (2018).
46. Mathew, J. S., Marcinauskas, L., Kalin, M., Kėželis, R., Kavaliauskas, Ž., Gecevičius, G., & Čapas, V. **Improvement of the Tribological Properties of Alumina Coatings by Zirconia Addition**, *Coatings* **11**, 991 (2021).
47. Koskilinna, J. O., Linnolahti, M. & Pakkanen, T. A. **Friction coefficient for hexagonal boron nitride surfaces from ab initio calculations**, *Tribology Letters* **24**, 37 (2006).
48. Rah, Y., Jin, Y., Kim, S. & Yu., K. **Optical analysis of the refractive index and birefringence of hexagonal boron nitride from the visible to near-infrared**, *Optics Lett.* **44**, 3797 (2019).
49. Franke, E., Schubert, M., Neumann, H., Tiwald, T. E., Thompson, D. W., Woollam, J. A., Hahn, J. & Richter, F. **Phase and microstructure investigations of boron nitride thin films by spectroscopic ellipsometry in the visible and infrared spectral range**, *J. Appl. Phys.* **82**, 2906 (1997).
50. Zhang, J., Sun, R., Ruan, D., Zhang, M., Li, Y., Zhang, K., Cheng, F., Wang, Z. & Wang, Z. M. **Point defects in two-dimensional hexagonal boron nitride: A perspective**, *J. Appl. Phys.* **128**, 100902 (2020).
51. Gottscholl, A., Diez, M., Soltamov, V., Kasper, C., Krauß, D., Sperlich, A., Kianinia, M., Bradac, C., Aharonovich, I. & Dyakonov, V. **Spin defects in hBN as promising temperature, pressure and magnetic field quantum sensors**, *Nat. Commun.* **12**, 4480 (2021).
52. Weston, L., Wickramaratne, D., Mackoite, M., Alkauskas, A., Van de Walle, C. G. **Native point defects and impurities in hexagonal boron nitride**, *Phys. Rev. B* **97**, 214104 (2018).

53. Sajid, A., Reimers, J. R., & Ford M. J. **Defect states in hexagonal boron nitride: Assignments of observed properties and prediction of properties relevant to quantum computation**, *Phys. Rev. B* **97**, 064101 (2018).
54. Sajid, A., Ford, M. J. & Reimers, J. R. **Single-photon emitters in hexagonal boron nitride: a review of progress**, *Rep. Prog. Phys.* **83**, 044501 (2020).
55. Caldwell, J. D., Aharonovich, I., Cassabois, G., Edgar, J. H., Gil, B. & Basov, D. N. **Photonics with hexagonal boron nitride**, *Nat. Rev. Mater.* **4**, 552–567 (2019).
56. Grosso, G., Moon, H., Lienhard, B., Ali, S, Efetov, D. K., Furchi, M. M., Jarillo-Herrero, P., Ford, M. J., Aharonovich, I. & Englund, D. **Tunable and high-purity room temperature single-photon emission from atomic defects in hexagonal boron nitride**, *Nat. Commun.* **8**, 705 (2017).
57. Sader, J. E., Borgani, R., Gibson, C. T., Haviland, D. B., Higgins, M. J., Kilpatrick, J. I., Lu, J., Mulvaney, P., Shearer, C. J., Slattery, A. D, Thorén, P., Tran, J., Zhang, H., Zhang, H. & Zheng, T. **A virtual instrument to standardise the calibration of atomic force microscope cantilevers**, *Rev. Sci. Instrum.* **87**, 093711 (2016).
58. Mescola, A., Paolicelli, G., Ogilvie, S. P., Guarino R., McHugh, J. G., Rota, A., Iacob, E., Gnecco, E., Valeri. S., Pugno, N. M., Gadhamshetty, V., Rahman M. M., Ajayan P., Dalton A. B. & M. Tripathi, M. **Graphene Confers Ultralow Friction on Nanogear Cogs**, *Small* **17**, 2104487 (2021).

Supplementary Information

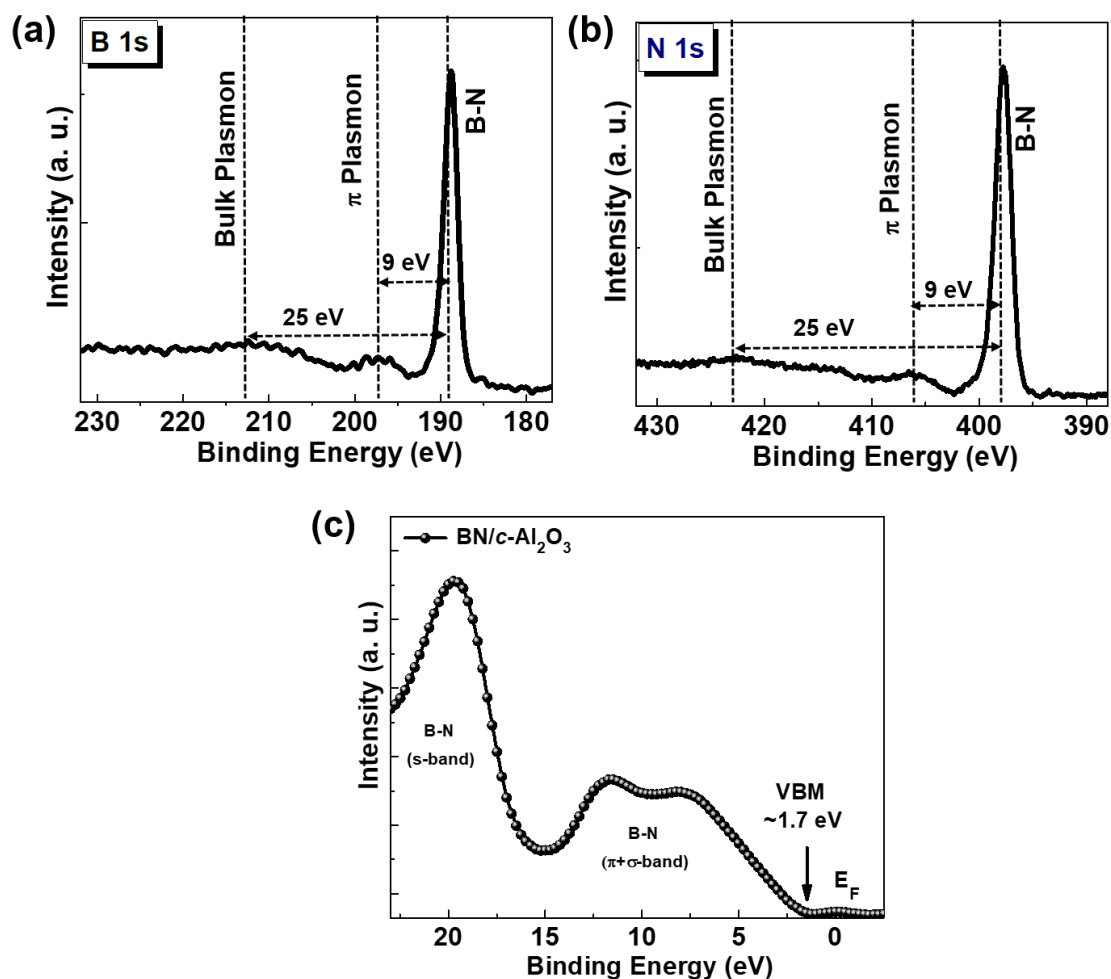


Fig. S1 (a), (b) XPS spectra of a room temperature grown BN film show the characteristic B-N bonding as well as the π -Plasmon and bulk Plasmon peaks of h-BN. (c) Valence band spectra (VBS) shows the characteristics feature of h-BN.

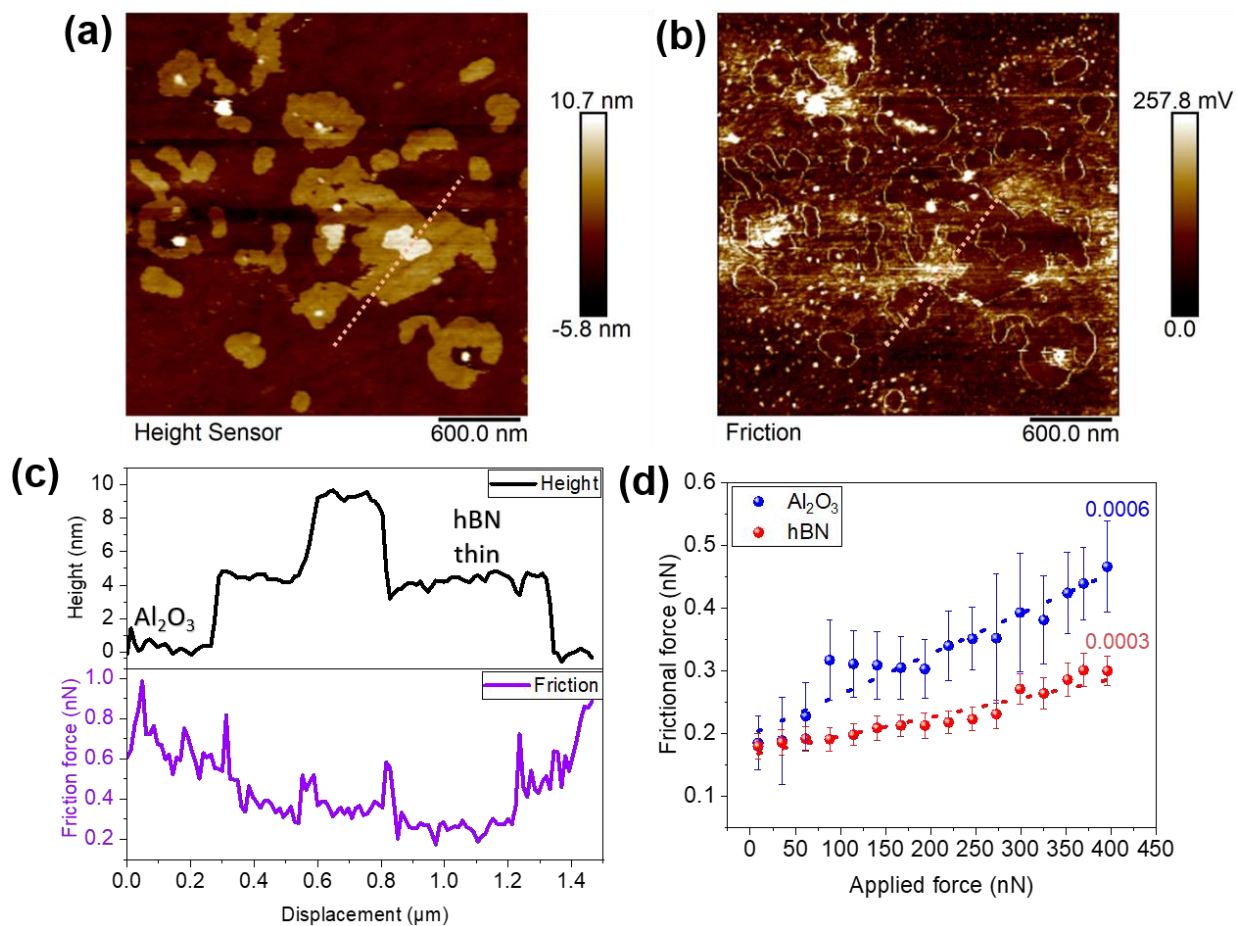


Fig. S2 (a) Topography (b) its corresponding frictional force map of h-BN/c-Al₂O₃. (c) Line profile of the height and the friction at the dotted line in panel (a) and (b). (d) Frictional force of the same region with different loading.

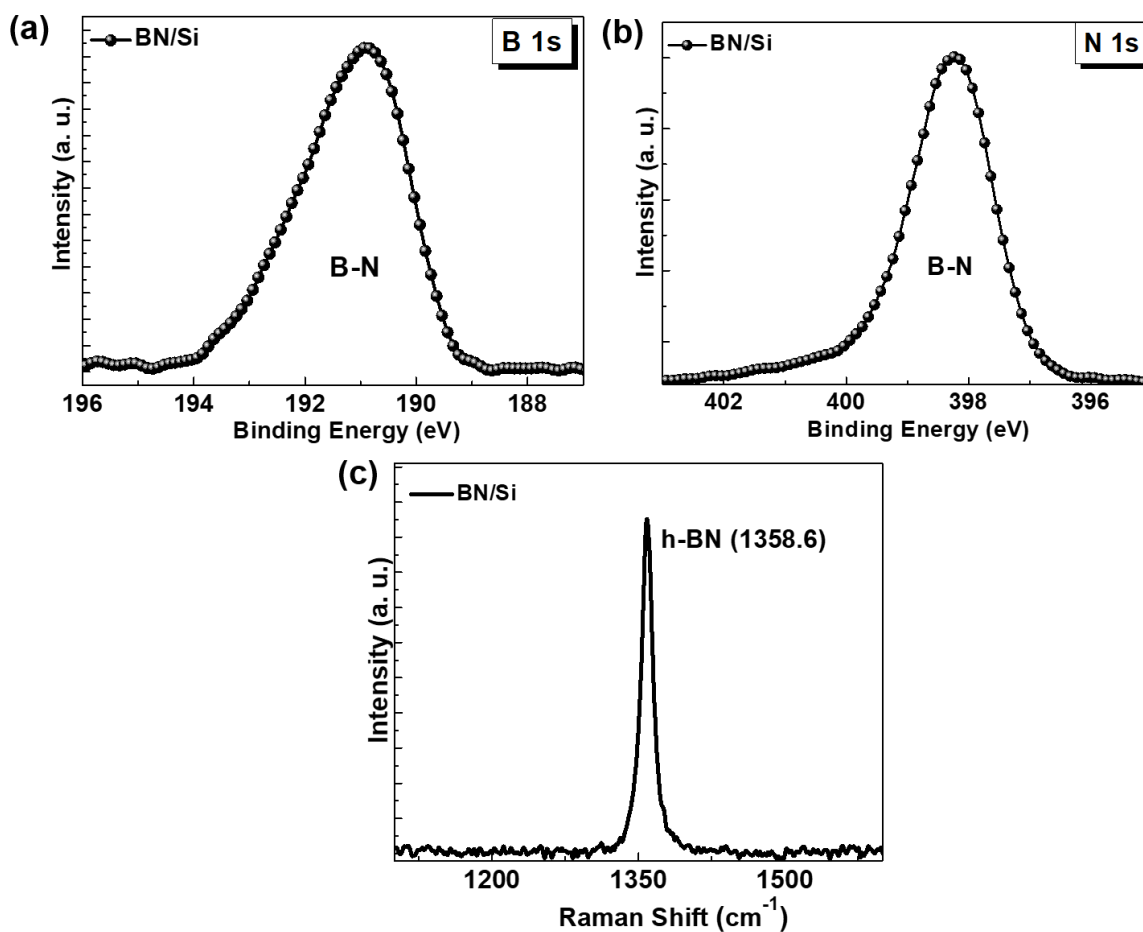


Fig. S3 | Characterizations of BN thin films grown on Si (100). (a), (b) XPS elemental B 1s and N 1s core scans confirms the presence of characteristics B-N bonds. (c) Raman spectra shows the peak at $\sim 1359 \text{ cm}^{-1}$, further confirming the growth of h-BN.

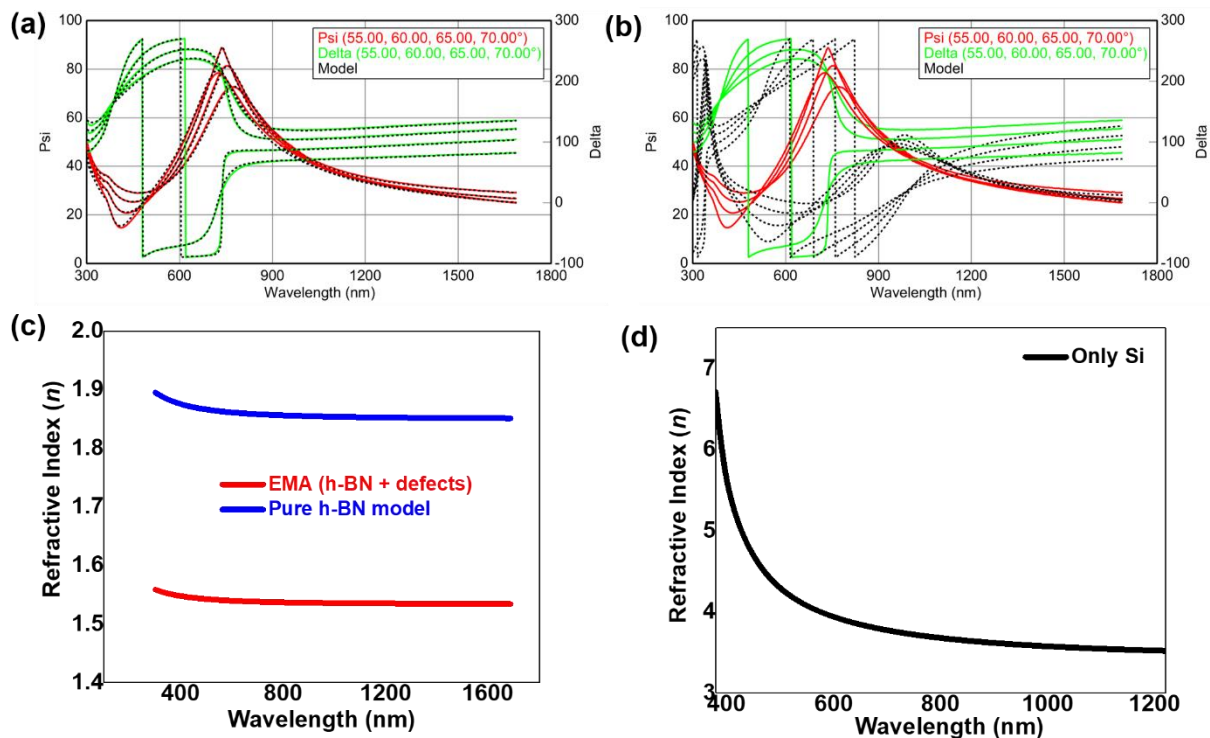


Fig. S4 (a)-(c) Fitting result comparison of different multilayer models used in h-BN film refractive index measurement. (a) Result of a three-layer model consisting of an effective approximation (EMA) layer on the two-layer reference model. (b) Result of a three-layer model consisting of the pure h-BN layer on the two-layer reference model. The h-BN with voids model provide a better fit with a much lower mean square error (MSE) of ~ 22.525 than for pure h-BN of ~ 685.652 . (c) Obtained RI with two different models. (d) Real part refractive index of Si substrate.